ACS APPLIED BIO MATERIALS

www.acsabm.org Article

Deep-Red and Near-Infrared Compact Cyanine Dyes for Sensitive NAD(P)H Sensing in Live Cells and Kidney Disease Tissues

Mahmood Norouzi, Adonis Amoli,* Yang Zhang, Yan Zhang,* Ashlyn Colleen Beatty, Anna Jarvi, Athar Ata,* Thomas Werner, and Haiying Liu*

Cite This: *ACS Appl. Bio Mater.* 2024, 7, 8552−8564 Read Online

ACCESS | Metrics & More | Article Recommendations | Supporting Information

ABSTRACT: Cyanine dyes constructed for NAD(P)H near-infrared sensing utilize extended π-conjugation but often exhibit delayed fluorescence responses to NAD(P)H due to reduced positive charge density in 3-quinolinium acceptors. This study introduces deep-red and near-infrared compact cyanine dyes represented by probes **A** and **B** for mitochondrial NAD(P)H detection in live cells. Probes **A** and **B** feature a unique structural design with a double bond connection linking 3-quinolinium to strategically positioned 1-methylquinolinium acceptor units at 2- and 4-positions, correspondingly. Probe **A** absorbs at 359 and 531 nm, while probe **B** absorbs at 324 and 370 nm, emitting subtle fluorescence at 587 and 628 nm, respectively, with no NADH present. Upon NADH exposure, probes **A** and **B** exhibit significant emission enhancements at 612 and 656 nm, correspondingly, attributed to the efficient reduction of 3-quinolinium units to electron-donative 1-methyl-1,4-dihydroquinoline units. Probe **B**, chosen for its near-infrared emission and fast response to NAD(P)H, effectively monitored dynamic intracellular NAD(P)H levels throughout diverse experimental conditions. In HeLa cells, minimal basal fluorescence increased upon NADH stimulation. It also identified increased NAD(P)H levels following chemical treatments with acesulfame potassium, cisplatin, carboplatin, and temozolomide, $CoCl_2$-induced hypoxia, and TLR4 activation in macrophages and in disease models of kidney pathology, where diseased tissues exhibited higher fluorescence than normal tissues. In fruit fly larvae under starvation conditions, probe **B** tracked NAD(P)H increases triggered by exogenous NADH, demonstrating its in vivo applicability for metabolic studies. These findings highlight probe **B**'s utility in elucidating dynamic NAD(P)H fluctuations in diverse biological contexts, offering insights into mitochondrial function and cellular metabolism.

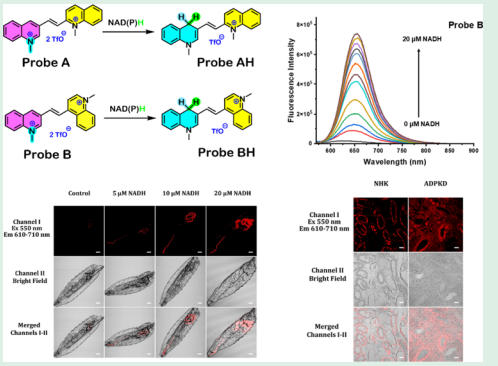

KEYWORDS: *cyanine dye, near-infrared imaging, NAD(P)H, kidney disease, fluorescent probes*

1. INTRODUCTION

Mitochondria are essential for driving cellular metabolism, acting as the powerhouse of the cell by orchestrating numerous biochemical processes, including oxidative phosphorylation and the regulation of cellular redox status.[1,2] Central to these metabolic pathways is NAD^+ (nicotinamide adenine dinucleotide) and its reduced state (NADH) along with their phosphorylated counterparts ($NADP^+$ and NADPH, respectively), which serve as crucial coenzymes involved in energy production, redox homeostasis, and various cellular signaling pathways.[3−8] Understanding the dynamics of these cofactors within the intricate milieu of live cells is essential for elucidating fundamental cellular processes and developing diagnostic and therapeutic strategies targeting metabolic disorders, cancer, and aging-related pathologies.[6−10] Recently, the development of fluorescent probes has revolutionized the study of cellular dynamics by providing live visualization and quantification of various biomolecules in live cells with high spatial and temporal resolution.[11−14] Among these probes, cyanine dyes have emerged as versatile tools for studying cellular processes due to their favorable photophysical properties, including high quantum yields, excellent photostability, and tunable absorption and emission spectra spanning the visible to near-infrared (NIR) regions.[11−17] Furthermore, their ability to selectively accumulate within mitochondria offers a unique opportunity to monitor the redox state of NAD(P)H directly within these organelles, providing insights into mitochondrial function and metabolic activity in live cells.[18−33] Near-infrared dyes tailored for NAD(P)H sensing leverage aromatic connection bridges integrated into cyanine dyes, significantly extending their π-conjugation. However, this approach inadvertently reduces the positive charge density of 3-quinolinium acceptors within the probes, thus slowing down

Received: September 17, 2024
Revised: November 9, 2024
Accepted: November 12, 2024
Published: November 26, 2024

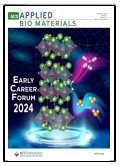

https://doi.org/10.1021/acsabm.4c01345
ACS Appl. Bio Mater. 2024, 7, 8552−8564

Scheme 1. Cyanine Dyes with Deep-Red and Near-Infrared Emissions for NAD(P)H Determination

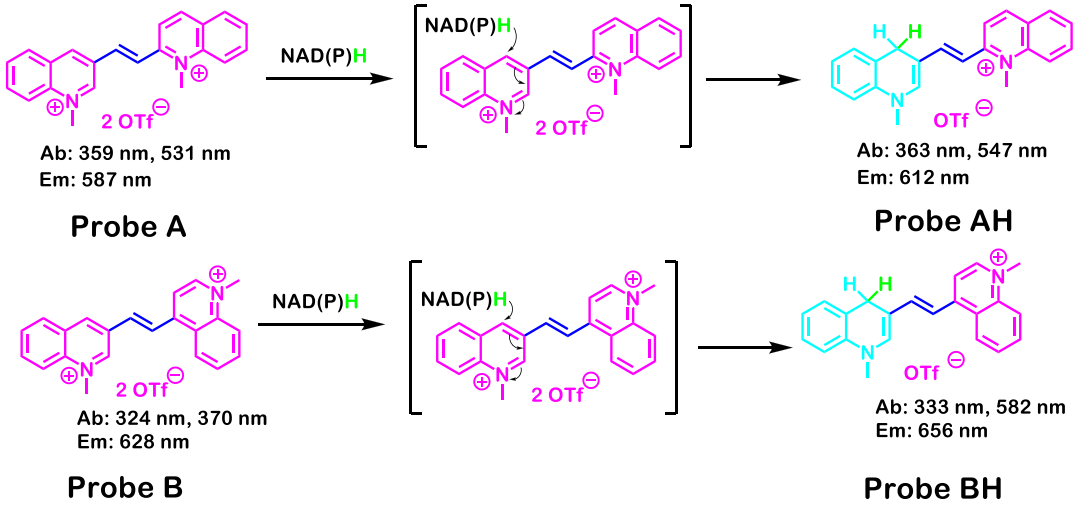

Scheme 2. Synthetic Approach for the Preparation of Cyanine Dyes for NAD(P)H Sensing Purposes

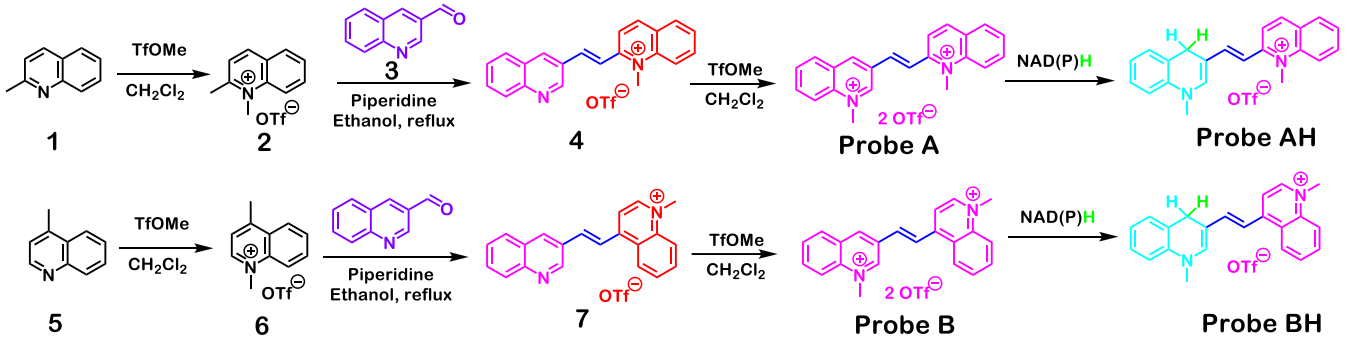

their fluorescence responses to NAD(P)H.[26,33] Addressing this, our study focuses on advancing deep-red and NIR compact cyanine dyes represented by probes **A** and **B** crafted to serve as fluorescence sensors for the detection of mitochondrial NAD(P)H in live cells (Scheme 1). Distinguished by their unique structural design, both probes **A** and **B** feature a double bond linkage bridge, linking 3-quinolinium to strategically positioned 1-methylquinolinium acceptor units at the 2-position and 4-position, correspondingly. Probe **A** reveals a peak absorption at 359 nm, with a subtle absorption at 531 nm with no NADH present, while probe **B** shows absorption peaks at 324 and 370 nm under similar conditions. In the lack of NADH, probes **A** and **B** emit faint emissions at 587 and 628 nm, correspondingly, owing to the presence of two electron-deficient acceptors, limiting intramolecular charge transfer. However, upon exposure to increasing NADH concentrations, probes **A** and **B** show remarkable fluorescence enhancements, manifesting distinct turn-on signals at 612 and 656 nm, correspondingly. This fluorescence intensity surge stems from the efficient reduction of 3-quinolinium units by NAD(P)H to 1-methyl-1,4-dihydroquinoline electron-providing units, generating well-structured cyanine dyes with acceptor-π-conjugated-donor systems. This configuration facilitates the intramolecular transfer from the 1-methyl-1,4-dihydroquinoline-donating group to the 1-methylquinolinium acceptor, elucidating the mechanism underlying the pronounced turn-on fluorescence observed in the probes. Fluorescent probe **B**, selected for its NIR emission and rapid kinetics in reaction to NAD(P)H, effectively monitored dynamic alterations in cellular NAD(P)H levels under various environments. In HeLa cells, minimal fluorescence was observed during control experiments, indicating low basal NAD(P)H levels, with a dose-dependent rise upon pretreatment with NADH. Real-time imaging demonstrated probe **B**'s rapid response to NADH in live cells. In response to chemical treatments, including acesulfame potassium exposure, cisplatin, carboplatin, and temozolomide treatment, $CoCl_2$-induced hypoxia, and TLR4 activation in macrophages, probe **B** consistently detected elevated NAD(P)H levels. Additionally, in models of kidney disease, probe **B** revealed significantly higher NAD(P)H fluorescence in diseased tissues versus healthy tissues, highlighting its sensitivity in detecting metabolic alterations. Furthermore, in fruit fly larvae subjected to starvation conditions, probe **B** effectively tracked increases in NAD(P)H levels triggered by exogenous NADH, demonstrating its utility in vivo for monitoring metabolic dynamics. These results collectively underscore probe **B**'s versatility in studying dynamic NAD(P)H fluctuations across different cellular and disease contexts.

2. EXPERIMENTAL SECTION

For more detailed information on the experiments, please refer to the Supporting Information.

2.1. Synthesis of Probe A. **^{1}H NMR** (DMSO-d_6, 500 MHz): δ 10.10 (1H, s), 9.66 (1H, s), 9.28 (1H, d, J = 9.0 Hz), 8.67 (1H, d, J = 9.0 Hz), 8.61−8.57 (2H, m), 8.54 (1H, t, J = 7.9 Hz), 8.46 (1H, t, J = 7.9 Hz), 8.37 (1H, t, J = 7.6 Hz), 8.33−8.27 (3H, m), 8.15 (1H, t, J = 7.6 Hz), 8.06 (1H, t, J = 7.5 Hz), 4.73 (3H, s), 4.68 (3H, s) ppm. **^{13}C NMR** (DMSO-d_6, 125 MHz): δ 154.96, 149.97, 145.61, 145.40,

https://doi.org/10.1021/acsabm.4c01345
ACS Appl. Bio Mater. 2024, 7, 8552−8564

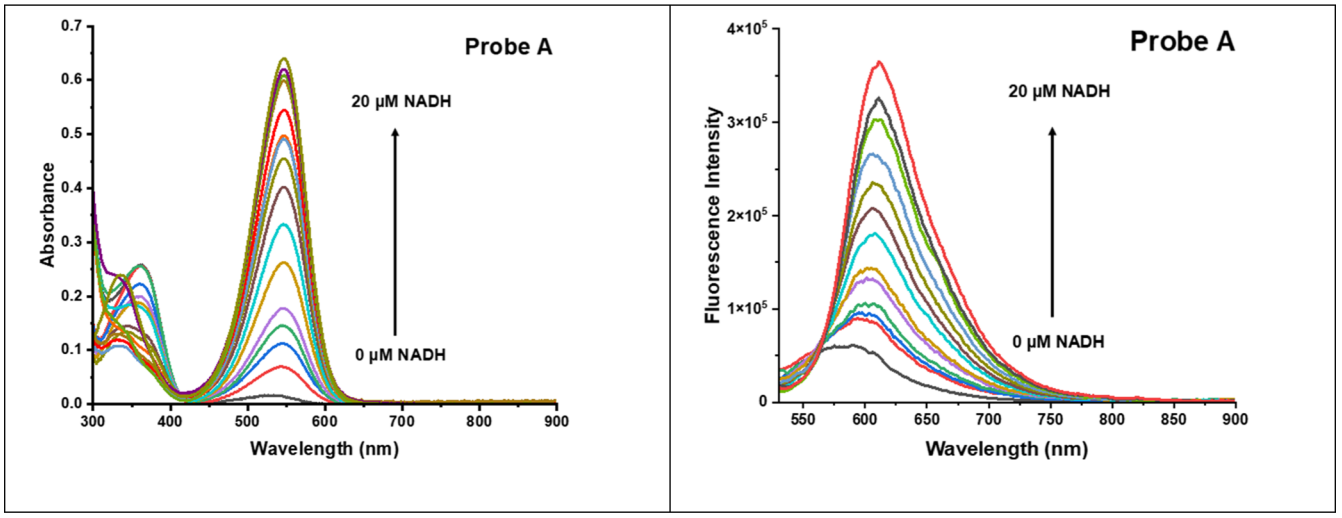

Figure 1. Optical spectra of probe **A** under both NADH-free and NADH-containing conditions in PBS buffers (pH 7.4) at room temperature under a 500 nm excitation.

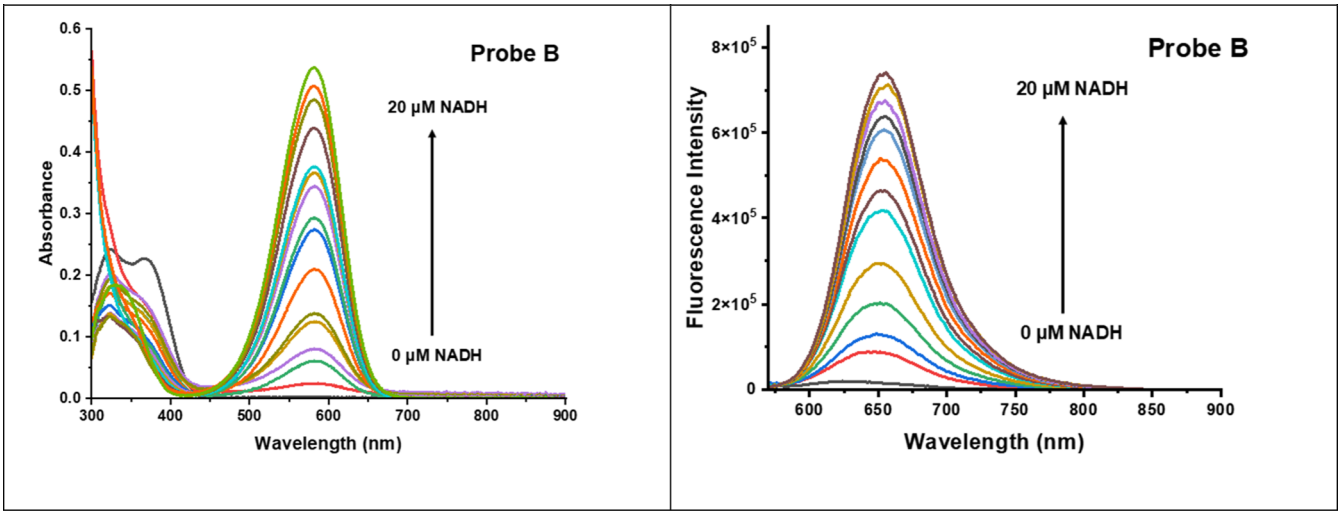

Figure 2. Optical spectra of probe **B** under both NADH-free and NADH-containing conditions in PBS buffers (pH 7.4) at room temperature under a 550 nm excitation.

139.41, 138.87, 138.07, 136.44, 135.58, 131.04, 130.80, 130.29, 128.83, 128.75, 128.54, 124.71, 121.94, 119.61, 119.50, 45.93, 40.57 ppm. **^{19}F NMR** (DMSO-d_6, 470 MHz): δ −77.75 ppm. **LC−MS** $C_{22}H_{20}N_2^+$, m/z; found, 156.25, calcd 156.08.

2.2. Synthesis of Probe B. 1H NMR (DMSO-d_6, 500 MHz): δ 10.13 (1H, s), 9.63 (1H, s), 9.53 (1H, d, J = 6.1 Hz), 9.02 (1H, d, J = 8.4 Hz), 8.72 (1H, d, J = 16.1 Hz), 8.60−8.51 (4H, m), 8.37−8.28 (3H, m),, 8.19 (1H, t, J = 7.5 Hz), 8.13 (1H, t, J = 7.6 Hz), 4.74 (3H, s), 4.64 (3H, s) ppm. 13C NMR (DMSO-d_6, 125 MHz): δ 150.94, 149.94, 149.11, 144.80, 138.88, 137.86, 136.09, 135.39, 135.22, 130.88, 129.89, 129.50, 128.95, 126.70, 126.09, 125.48, 121.94, 119.82, 119.44, 117.54, 45.90, 45.25 ppm. 19F NMR (DMSO-d_6, 470 MHz): δ −77.75 ppm. LC−MS C22$H_{20}N_2^+$, m/z; found, 156.17, calcd 156.08.

3. RESULTS AND DISCUSSION

3.1. Synthetic Approaches. In pursuit of the main goal of crafting highly responsive sensors for detecting NAD(P)H, an innovative platform was devised by fusing a quinolinium-sensing component with cyanine dyes. This involved the synthesis of a distinct acceptor-π-acceptor architecture with diminished fluorescence via a straightforward chemical condensation process. The starting components, 3-quinolinecarboxaldehyde (**3**), along with either 1,2-dimethylquinolinium iodide (**2**) or 1,4-dimethylquinolinium iodide (**6**), underwent condensation, yielding pivotal intermediates **4** and **7** (Scheme 2). Following this, the quinoline segments of these compounds were subjected to methylation, as illustrated in Scheme 2. Utilizing this methodology, two sensitive probes were adeptly engineered and produced, showcasing remarkable sensitivity and selectivity in NAD(P)H detection (Scheme 2). Comprehensive analysis of both probes and intermediates was conducted through NMR and mass spectrometry techniques. The products formed (probes **AH** and **BH**) from the interaction of the probes with NADH were also characterized by mass spectrometric analysis.

3.2. NADH-Induced Optical Responses of the Probes. Probe **A** reveals a weak peak absorbance at 531 nm and a moderate-intensity absorption maximum at 359 nm, along with a weak fluorescence peak at 587 nm when NADH is not present in PBS buffer (pH 7.4) (Figure 1). In comparison, probe **B** shows absorption features at 370 and 324 nm, alongside a minimal fluorescence peak at 628 nm under the

https://doi.org/10.1021/acsabm.4c01345
ACS Appl. Bio Mater. 2024, 7, 8552−8564

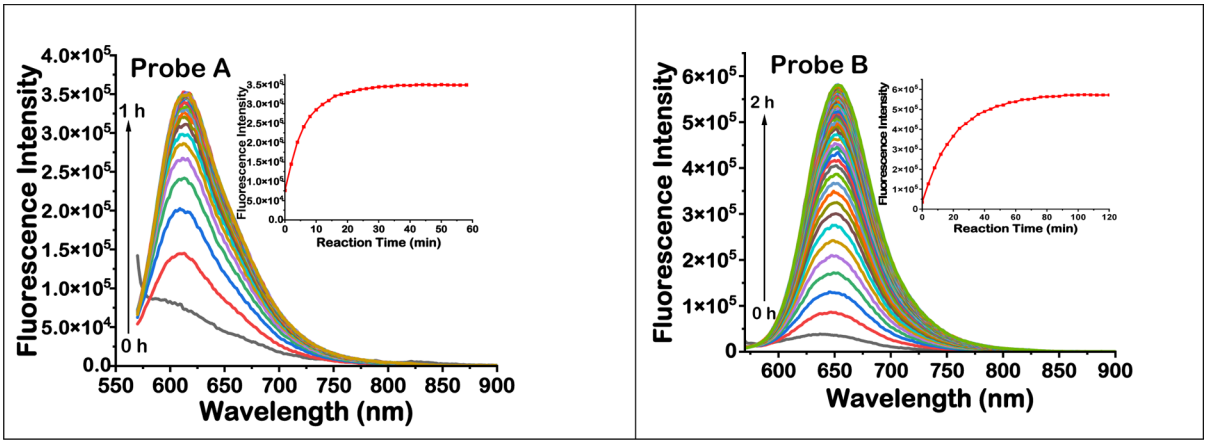

Figure 3. Emission spectra of the probes with 15 μM NADH in PBS buffers (pH 7.4) under 500 nm (probe **A**) and 550 nm (probe **B**) excitation at different reaction times.

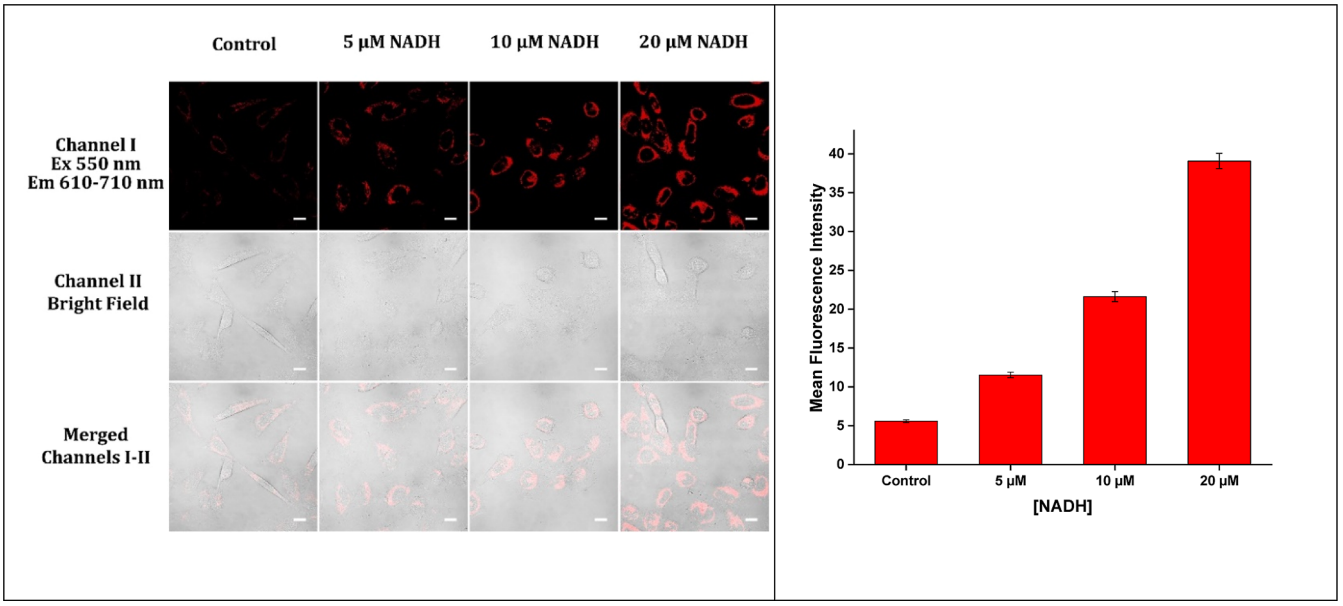

Figure 4. Cellular emission images of HeLa cells, initially exposed to varying NADH concentrations in glucose-absent DMEM for 30 min, followed by exposure to 5 μM probe **B** in glucose-absent DMEM for an extra 20 min. Emission signals were detected, and emissions were collected within the 610−710 nm emission range under an excitation of 550 nm. Scale bar: 50 μm.

same conditions (Figure 2). Probe **A** presents a clear absorption response to increasing NADH concentrations, demonstrated by enhanced absorption at 531 nm. This is accompanied by a significant fluorescence turn-on at 612 nm, with a noticeable red shift from 587 to 612 nm as NADH concentrations increase from 0 to 20 μM (Figure 1). Similarly, probe **B** shows absorption changes with rising NADH levels, characterized by the appearance and enhanced absorption at 550 nm. It also exhibits a pronounced fluorescence turn-on at 656 nm, with a red shift from 628 to 656 nm as NADH concentrations increase from 0 to 20 μM (Figure 2). The weak fluorescence observed in probes **A** and **B** can be attributed to the fluorescence quenching effect, which occurs in the absence of intramolecular charge transfer (ICT) owing to the two electron-withdrawing acceptor groups: 3-quinolinium and 1-methylquinolinium within the cyanine platforms. Upon interaction with NADH, the fluorescence of the probes is significantly enhanced. This turn-on fluorescence response is due to an efficient ICT from the 1-methyl-1,4-dihydroquinoline donor to the 1-methylquinolinium acceptor within the cyanine framework. NADH effectively reduces the 3-quinolinium electron acceptor to a 1-methyl-1,4-dihydroquinoline electron donor, resulting in the formation of distinct donor-π-acceptor (D-π-A) cyanine fluorophores (Scheme 1).

Probes **A** and **B** present quick fluorescence responses to NADH, achieving steady-state fluorescence within 20 and 60 min, respectively (Figure 3). This quick response is due to the high charge density of the 3-quinolinium acceptor, which is connected to the 1-methylquinolinium acceptor units at the 2-position and 4-position via a double connection bridge. This structural configuration enhances the efficient NADH-triggered reduction of the 3-quinolinium electron-deficient acceptor, resulting in the formation of the 1-methyl-1,4-dihydroquinoline electron-supplying donor. The probes' reduced products, **AH** and **BH** (Scheme 1), were confirmed through mass spectrometry (Figures S17 and S18).

3.3. Selectivity, Photostability, and Cytotoxicity of the Probes. Photostability is crucial for the sustained

https://doi.org/10.1021/acsabm.4c01345
ACS Appl. Bio Mater. 2024, 7, 8552−8564

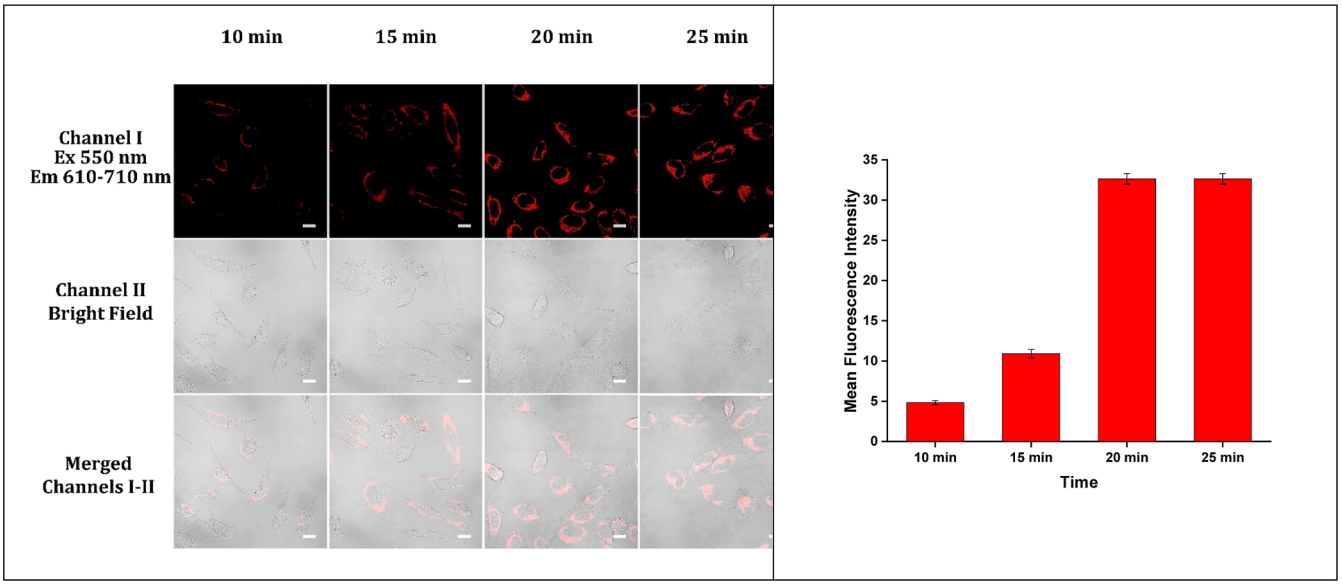

Figure 5. Cellular emission images representing the fluorescence response of probe **B** to intracellular NADH in live HeLa cells. Cells were pre-exposed to 5 μM probe **B** in glucose-lacking DMEM with 20 mM glucose concentration for varying durations. Fluorescence signals were detected using a 550 nm excitation and captured within the 610−710 nm emission range. Scale bar: 50 μm.

fluorescence of fluorophores during prolonged light exposure, ensuring reliable performance. Probes **A** and **B** exhibit outstanding photostability, showing minimal fluorescence changes even after continuous excitation at 500 and 550 nm for 1 and 2 h each, respectively. This feature is essential for applications requiring extended or repetitive imaging sessions as it mitigates the risk of photobleaching, which can otherwise distort signal stability and image consistency (Figures S21 and S22).

Probes **A** and **B** exhibit extraordinary specificity for NAD(P)H when compared with a variety of other substances. These include various cations (K^+, Na^+, Co^{2+}, Ca^{2+}, and Fe^{3+}), anions (HSO_3^-, SO_4^{2-}, CN^-, NO_2^-, NO_3^-, and Cl^-), biomolecules including cysteine and glutathione, amino acids like methionine and lysine, as well as carbohydrates such as fructose, glucose, lactate, and galactose. This remarkable level of probe selectivity is pivotal for the sensitive detection and measurement of NAD(P)H, a fundamental coenzyme critical for metabolic activities and a range of cellular functions (Figures S23 and S24).

An MTT reduction assay test was carried out to gauge the probe cytotoxicity, following established procedures. Probe **A** or **B** was applied to HeLa cells, and the transformation of the MTT dye into formazan was tracked, indicating mitochondrial enzymatic activity and cell viability.[34−39] These results demonstrated that the cell viability stayed above 86 or 90% even at a concentration of 40 μM for probe **A** or **B**, respectively, suggesting minimal impact on cell viability. The use of these low-cytotoxicity probes is crucial to minimize potential disruptions to cellular processes, ensuring the reliability of experimental outcomes. Furthermore, their low toxicity allows for extended exposure periods and repeated measurements, facilitating longitudinal studies and assessment of treatment responses with greater accuracy (Figure S25).

3.4. Fluorescence Cellular Imaging of NAD(P)H in Living Cells. Because of its near-infrared emission and quick reaction to NAD(P)H, probe **B** was chosen to monitor NAD(P)H level dynamics in cells resulting from different chemical treatments. To affirm probe **B**'s specificity for intracellular NAD(P)H, HeLa cells were pretreated with control or various NADH concentrations for 30 min, and further, cells were incubated with 5 μM probe **B** in glucose-absent DMEM for 30 min. As Figure 4 shows, cells in the control group exhibited minimal fluorescence, implying a low baseline level of intrinsic NAD(P)H and the inactivity of probe **B** with NADH levels remaining low. On the contrary, HeLa cells pre-exposed to various NADH concentrations displayed a dose-responsive augmentation in emission (Figure 4), verifying probe **B**'s specificity for quantifying intracellular NADH levels. Our results confirm probe **B**'s ability to specifically track dynamic changes in NADH levels. The strong correlation between probe **B**'s fluorescence and NADH levels enables reliable quantitative imaging.

To measure the real-time fluorescence of probe **B** in response to NADH in live cells, HeLa cells were pre-exposed to 5 μM probe **B** in glucose-absent DMEM with 20 mM glucose for varying durations (Figure 5). The emission intensity of HeLa cells is enhanced in a time-dependent manner from 10 to 25 min with stable levels at 25 min. This rapid response suggests that probe **B** efficiently detects NADH dynamics in live cells at physiological temperature (37 °C), contrasting its response in a cuvette at room temperature (Figures 5 and 3). These results demonstrate that probe **B** provides fast and reliable fluorescence responses to changes in NADH levels within live cells. This capability is essential for studying dynamic metabolic processes, where real-time monitoring of NADH fluctuations can provide insights into cellular metabolism and function. The comparison with cuvette experiments underscores the responsiveness of probe **B** under physiological conditions, reinforcing its utility for studying intracellular NADH dynamics in a biologically relevant context.

3.5. Mitochondrial Targeting of Probe B in HeLa Cells. To assess the mitochondrial targeting capability of probe **B** in live HeLa cells, a colocalization experiment was performed using MitoView 405, a mitochondrial marker.[31,33,36,37,40−42] The cells were initially exposed to 20 mM glucose in glucose-

https://doi.org/10.1021/acsabm.4c01345
ACS Appl. Bio Mater. 2024, 7, 8552−8564

absent DMEM for 30 min and subsequently treated with 5 μM probe **B** and MitoView 405 for another 20 min in glucose-absent DMEM. Fluorescence imaging was conducted with probe **B** excited at 550 nm, capturing emissions between 610 and 710 nm (channel I), while MitoView 405 was under 405 nm excitation and emitted signals were detected between 425 and 475 nm. The obtained images (Figures 6 and S1) show a high degree of concurrent localization between MitoView 405 and probe **B**, with a Pearson correlation coefficient of 0.948. This strong correlation indicates that probe **B** predominantly localizes within the mitochondria. The results confirm that probe **B**, which carries two positive charges, effectively targets mitochondria in live cells. This targeting is likely facilitated by the probe's positive charges, which allow it to interact with the negatively charged mitochondrial membrane potential. The high Pearson correlation coefficient underscores the precision with which probe **B** can localize to mitochondria, making it a promising tool for mitochondrial imaging. These findings demonstrate that probe **B** can be used to study mitochondrial dynamics and function with high specificity. The excellent colocalization with MitoView 405 suggests that probe **B** could be valuable for further research into mitochondrial processes, potentially providing insights into mitochondrial bioenergetics, dynamics, and pathology in various cellular environments.

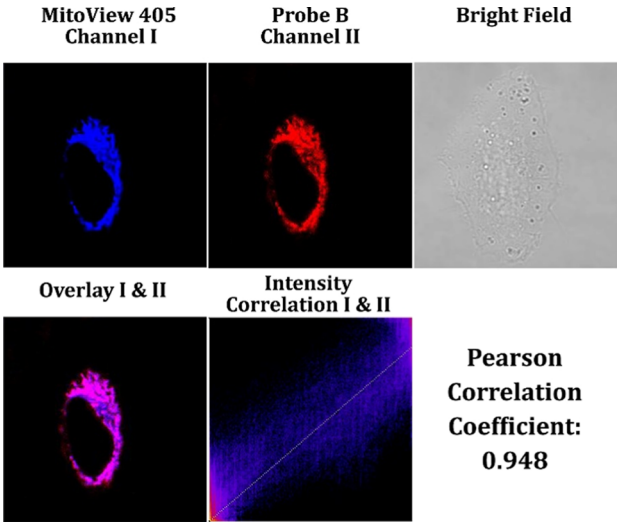

Figure 6. Emission imaging of HeLa cells initially treated with 20 mM glucose in glucose-absent DMEM for 30 min, subsequently coincubated for 20 min with 5 μM MitoView 405 and 5 μM probe **B** in the same medium. Fluorescence imaging was taken with a 550 nm excitation, and emissions were recorded from 610 to 710 nm for channel I. MitoView 405 was stimulated at 405 nm, with the resulting emissions recorded in the 425 to 475 nm range. Scale bar: 20 μm.

Acesulfame potassium, commonly known as Ace-K, is a synthetic sweetener that is about 200 times sweeter than sucrose (table sugar).[43−45] It is extensively used in a range of food and beverage items, encompassing sweets, gum, soft drinks, pastries, and dairy foods. Ace-K was discovered in 1967 and granted FDA (the U.S. Food and Drug Administration) approval in 1988.[43−45] To assess the Ace-K impact on cellular metabolism, a study was conducted using HeLa cells and probe **B**. In this study, HeLa cells were exposed to diverse Ace-K concentrations and then incubated with probe **B**. The results highlighted a substantial enhancement in cellular emission, suggesting elevated NAD(P)H levels following Ace-K administration (Figure 7). This increase occurred even in a culture medium lacking glucose, implying several possible mechanisms. These mechanisms might include the activation of different metabolic routes that enhance NAD(P)H generation, the stimulation of enzymes associated with the tricarboxylic acid cycle, and the activation of cellular stress reactions that lead to the activation of NAD(P)H synthetic pathways to maintain redox balance.[46,47] Moreover, Ace-K might impact intracellular signaling mechanisms like the AMP-activated protein kinase pathway.[48] These outcomes spotlight the complicated interconnections between cellular metabolic functions, stress mechanisms, and signaling pathways modulated by Ace-K administration.

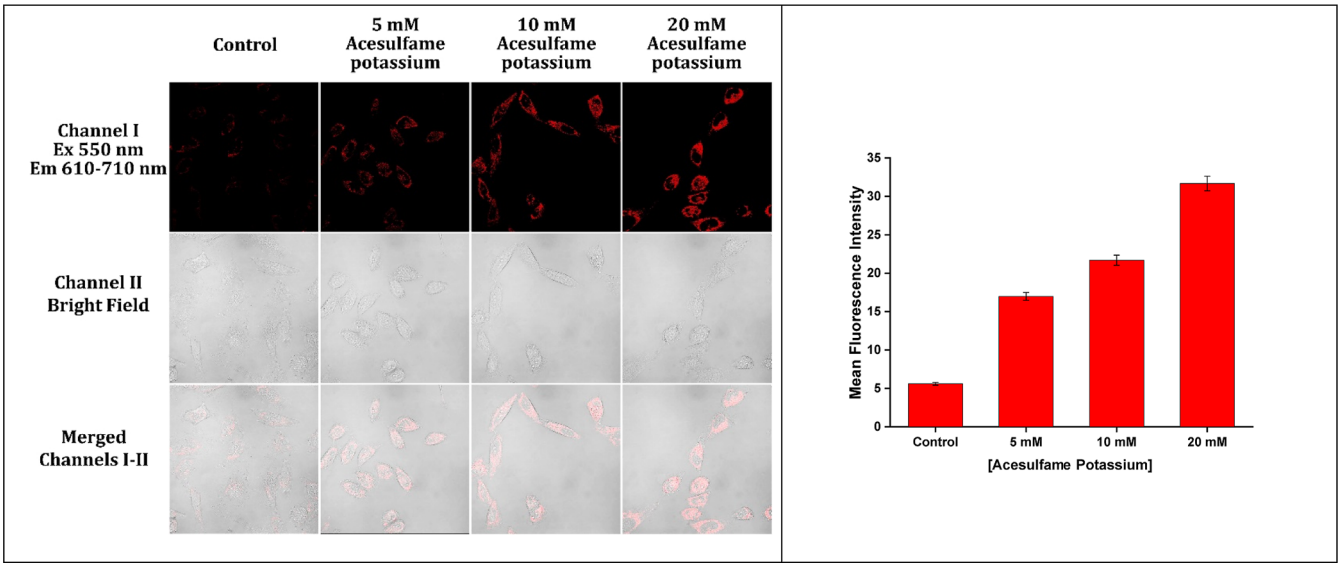

Figure 7. Cellular images of HeLa cells treated with Ace-K for 30 min in glucose-deficient DMEM and subsequently administered with 5 μM probe **B** for an extra 20 min. Fluorescence was observed using a 550 nm excitation wavelength, and emissions were gathered in the 610−710 nm range. Scale bar: 50 μm.

https://doi.org/10.1021/acsabm.4c01345
ACS Appl. Bio Mater. 2024, 7, 8552−8564

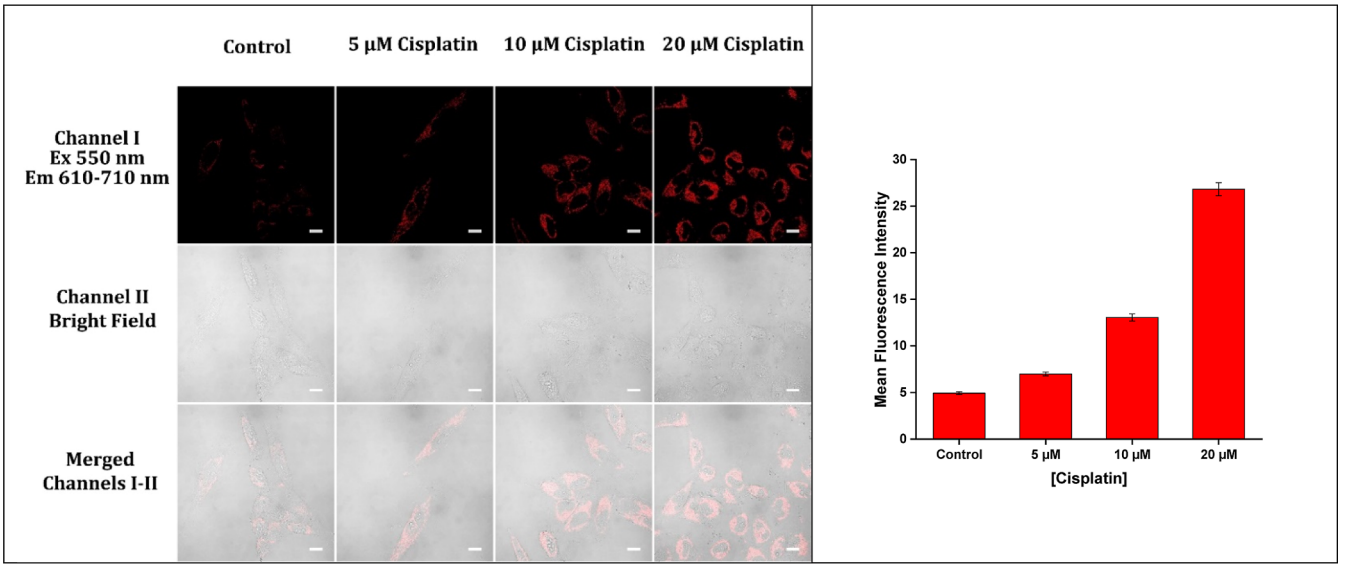

Figure 8. Emission images of HeLa cells pretreated with different cisplatin concentrations in glucose-absent DMEM for 30 min, which further underwent 20 min exposure to 5 μM probe **B** in glucose-absent DMEM. Emission was observed under a 550 nm excitation, and emissions were gathered between 610 and 710 nm. Scale bar: 50 μm.

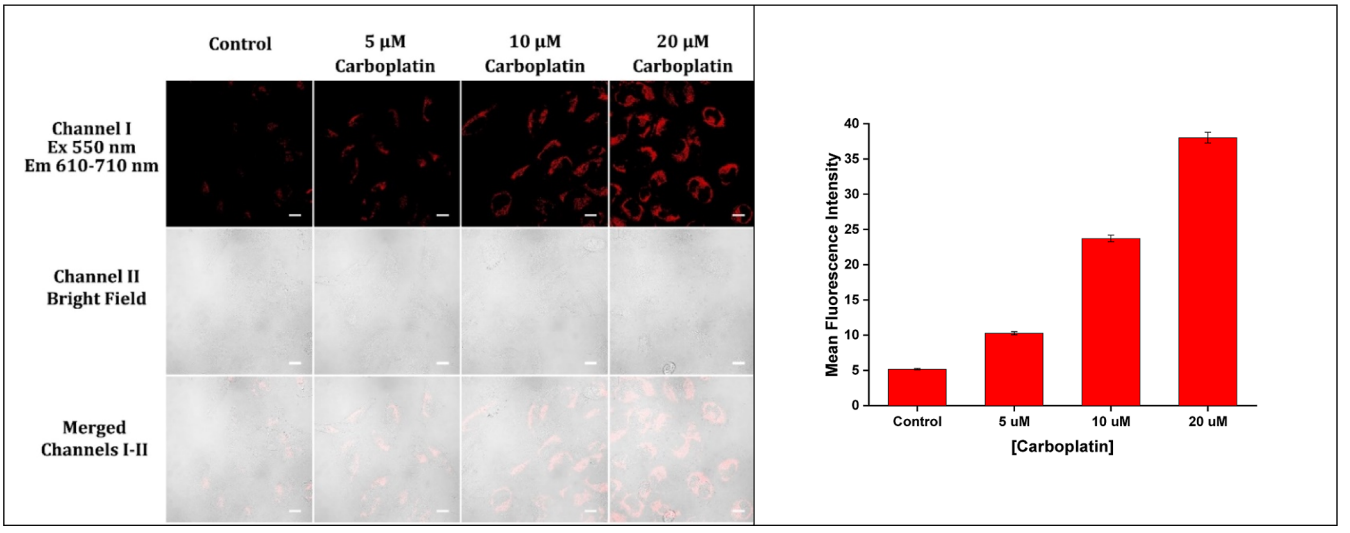

Figure 9. Emission images of HeLa cells after a 30 min pre-exposure to diverse carboplatin in glucose-absent DMEM, which further underwent a 20 min exposure to 5 μM probe **B** in glucose-absent DMEM. Emission was observed under a 550 nm excitation, and emissions were recorded in the 610−710 nm range. Scale bar: 50 μm.

Cisplatin is a widely utilized chemotherapeutic agent in treating various cancers, such as ovarian, testicular, bladder, and head and neck cancers.[49−51] It exerts its anticancer effects primarily through cross-linking of DNA, inducing DNA damage and triggering apoptosis in cells with high proliferation rates.[49−51] Additionally, cisplatin-induced cell damage is linked to the generation of reactive oxygen species and the onset of oxidative stress, which can impact cellular metabolic pathways, including those involving nicotinamide adenine dinucleotide.[49−51] In this study, various cisplatin concentrations (0, 5, 10, and 20 mM) were administered to HeLa cells for 30 min to explore their influence on NAD(P)H levels, monitored with probe **B** (Figure 8). There was a concentration-dependent enhancement in emission intensity, suggesting rising NAD(P)H levels corresponding to higher cisplatin concentrations. This NAD(P)H increase can arise from several mechanisms. Cisplatin-induced oxidative stress leads to increased ROS production, prompting cells to enhance their antioxidant defenses, often involving upregulation of NAD(P)H-dependent enzymes and increased NAD(P)H production. Moreover, cisplatin treatment can result in metabolic reprogramming, where cancer cells increase glycolysis and the pentose phosphate pathway activity, both generating NAD(P)H as a byproduct. Besides, DNA damage from cisplatin brings about the activation of repair enzymatic mechanisms dependent on NAD(P)H as a cofactor involved in base excision and nucleotide excision repair.[49−51] The detected rise in NAD(P)H levels upon cisplatin treatment reveals that cells mount a multifaceted response to mitigate the drug's cytotoxicity. This response includes bolstering antioxidant defenses, altering metabolic pathways, and repairing DNA damage, all crucial for cell survival and function under stress conditions. Understanding these biochemical and cellular responses to cisplatin provides insight into its mechanism of action and highlights

https://doi.org/10.1021/acsabm.4c01345
ACS Appl. Bio Mater. 2024, 7, 8552−8564

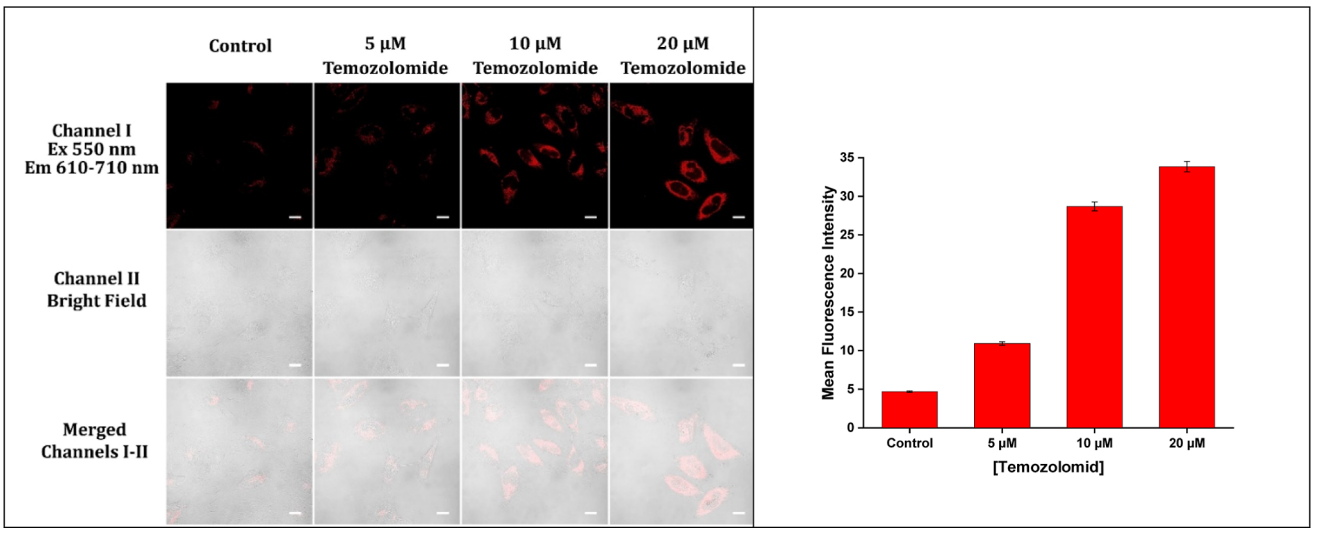

Figure 10. Emission images of HeLa cells after a 30 min pre-exposure to diverse temozolomide concentrations in glucose-lacking DMEM, followed by a 20 min coculturing with 5 μM probe **B** in glucose-absent DMEM. Emission was observed with a 550 nm excitation, and emissions were gathered in the 610−710 nm range. Scale bar: 50 μm.

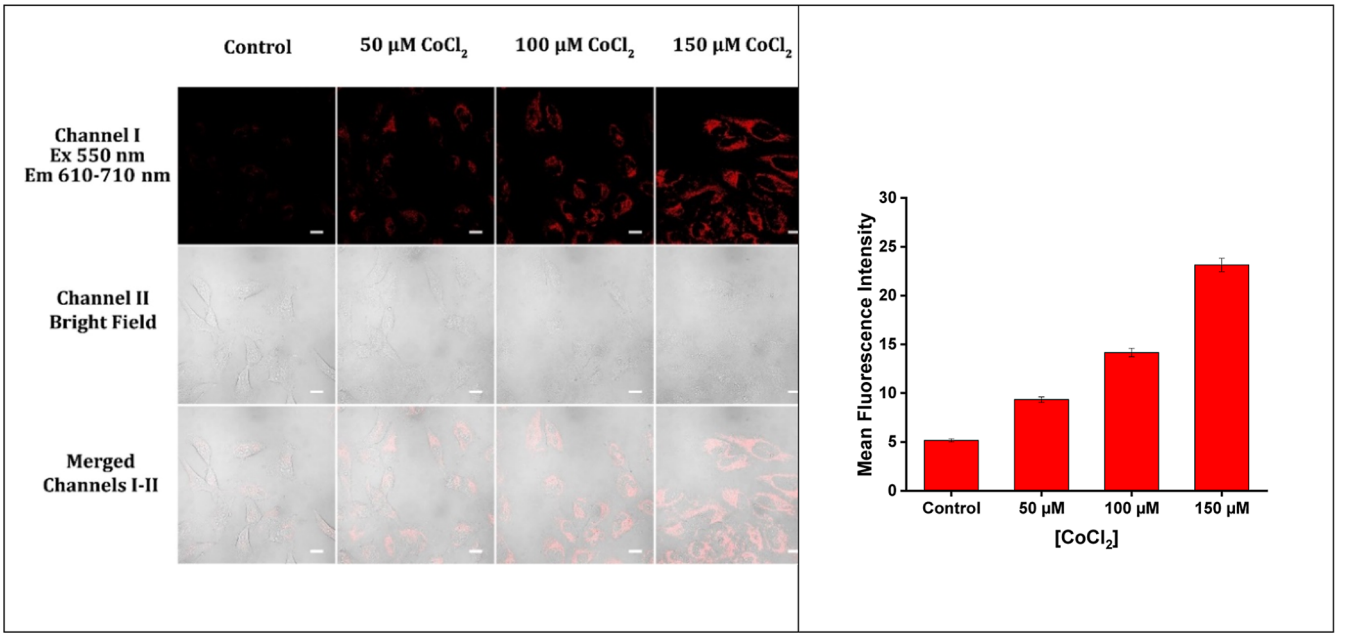

Figure 11. Emission images of HeLa cells after a 30 min pre-exposure to diverse $CoCl_2$ concentrations in glucose-absent DMEM, followed by a 20 min exposure to 5 μM probe **B** in glucose-lacking DMEM. Emission was observed with a 550 nm excitation, and emissions were gathered in the 610−710 nm range. Scale bar: 50 μm.

potential targets for enhancing its therapeutic efficacy or mitigating its side effects.

Carboplatin, a chemotherapy drug widely used to treat various cancers, functions as a platinum-based agent that causes DNA cross-linking and disrupts cellular replication.[52−55] To assess the influence of carboplatin on NAD(P)H levels within HeLa cells, the cells were exposed to various carboplatin doses for 30 min and then to 5 μM probe **B** for 20 min. Figure 9 illustrates that the control group (0 mM) had minimal baseline emission, whereas cells exposed to 5, 10, and 20 μM carboplatin displayed a dose-dependent enhancement in emission signals. The rise of NAD(P)H levels seen after receiving carboplatin can be ascribed to several factors. As carboplatin induces DNA damage, cells may increase their metabolic activity to repair the damage, leading to an upregulation of pathways such as glycolysis alongside the pentose phosphate pathway, both of which contribute to increased NADH production.[52−55] Additionally, the drug may cause oxidative stress and mitochondrial dysfunction, resulting in altered electron transport chain activity and accumulation of NADH. The augmentation of NAD(P)H levels reflects these metabolic shifts as cells adapt to the stress induced by carboplatin.

Temozolomide, an alkylating agent commonly used in the treatment of glioblastoma and other cancers, functions by triggering DNA damage and disrupting cellular processes.[56−59] In this work, we examined its effect on NAD(P)H levels in HeLa cells using probe **B**. As depicted in Figure 10, the control

https://doi.org/10.1021/acsabm.4c01345
ACS Appl. Bio Mater. 2024, 7, 8552−8564

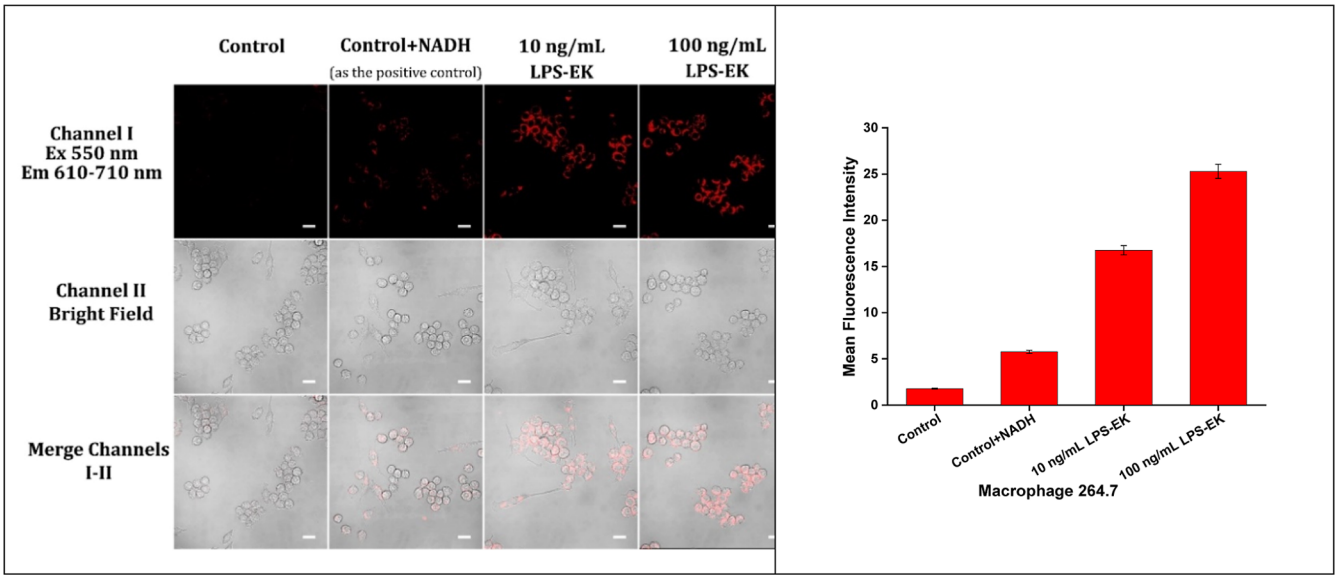

Figure 12. Cellular emission image of Raw 264.7 macrophage cells depicting the effects of TLR4 activation on levels of NAD(P)H in macrophages. Raw 264.7 macrophage cells were exposed to 0.01% H_2O as a vehicle control (control) or to different concentrations of LPS-EK, a specific TLR4 agonist, for 30 min, and proceeded with exposure to 5 μM probe **B** for 20 min. NADH-incubated cells were utilized as the positive control. Fluorescence was observed using a 550 nm excitation wavelength, and emissions were documented in the 610−710 nm range. Scale: 50 μm.

group exhibited baseline fluorescence, while cells exposed to different concentrations of temozolomide showed a correlated increase in emission signals. The surge in NAD(P)H levels observed with temozolomide treatment can be ascribed to the drug's impact on cellular metabolism. As an alkylating agent, temozolomide induces DNA damage, which can lead to a heightened metabolic response as the cell attempts to repair the damage.[56−59] This metabolic shift often results in increased glycolytic activity and a corresponding rise in NADH production.[56−59] Furthermore, temozolomide can cause mitochondrial dysfunction, which disrupts the electron transport chain and causes NADH accumulation.[56−59] This ascent in NAD(P)H levels may reflect these metabolic changes as cells increase their reducing equivalents to counteract oxidative stress and maintain cellular homeostasis.[56−59] These results highlight probe **B**'s potential as a sensitive NAD(P)H level indicator triggered by chemotherapeutic treatments. Monitoring variations in NAD(P)H levels brings significant insight into the cellular mechanisms underlying drug action as well as the metabolic adaptations of cancer cells. Further studies are warranted to explore the detailed metabolic pathways involved and the implications for optimizing cancer therapy.

Hypoxia is a well-known stress condition that significantly impacts cellular metabolism and the redox state.[60,61] $CoCl_2$ is commonly used as a hypoxia-mimicking agent because it stabilizes hypoxia-inducible factors (HIFs) by inhibiting prolyl hydroxylases, thereby simulating hypoxic conditions even in the presence of normal oxygen levels.[62,63] Hypoxia leads to the upregulation of glycolysis, generating NADH and NADPH. The increased NADH is a critical cofactor in glycolysis, which becomes the primary source of ATP under hypoxic conditions due to the limited function of oxidative phosphorylation.[62,63] NADPH is also vital for sustaining cellular redox balance and is integral to biosynthetic reactions and the detoxification of reactive oxygen species (ROS). Under hypoxic stress, cells enhance NADPH production pathways, such as the pentose phosphate pathway, to counteract oxidative stress and support anabolic reactions. In our study, we utilized $CoCl_2$ to induce hypoxic conditions in HeLa cells and employed fluorescent probe **B** to monitor cellular NAD(P)H level variations. We observed that $CoCl_2$ exposure brought about an ascent in NAD(P)H levels, evidenced by a rise in cellular emission intensity with enhancing concentrations of $CoCl_2$. This observation aligns with the metabolic adaptations seen under hypoxic conditions. The elevated fluorescence intensity detected by probe **B** reflects the higher intracellular concentrations of these cofactors (Figure 11). This NAD(P)H level rise is likely due to metabolic reprogramming that favors glycolysis and increased NADPH synthesis pathways under hypoxic conditions induced by $CoCl_2$ treatment. This finding is consistent with the known cellular response to hypoxia, where metabolic shifts enhance the production of NADH and NADPH to support energy production and maintain redox homeostasis. The use of fluorescent probe **B** provided a reliable and sensitive method to monitor these changes, offering insights into the cellular metabolic adjustments during hypoxic stress.

Toll-like receptor 4 (TLR4) is pivotal in regulating innate immune responses by identifying pathogen- and damage-related molecular patterns.[64,65] Upon activation in macrophages, TLR4 induces metabolic changes, prominently affecting NADH and NADPH levels, vital indicators of cellular redox state and metabolic activity.[64,65] To investigate whether probe **B** can monitor NAD(P)H levels induced by TLR4 activation in immune cells, Raw 264.7 macrophages were treated with LPS-EK, a potent and specific TLR4 agonist, for 30 min, then incubated with probe **B**, and subjected to fluorescence microscopy and spectroscopy. Our immunoblot analysis showed that LPS-EK treatment remarkably increased the phosphorylation of IκBα, the inhibitor of NF-κB, and induced its subsequent degradation in Raw 264.7 macrophages, demonstrating that LPS-EK successfully stimulated cellular innate immune responses. We discovered that LPS-EK robustly raised NAD(P)H levels in a concentration-related manner in Raw 264.7 cells (Figure 12). Our study underscores that TLR4 activation induces a substantial increase in cellular

https://doi.org/10.1021/acsabm.4c01345
ACS Appl. Bio Mater. 2024, 7, 8552−8564

NADH and NADPH levels in macrophages, as detected by fluorescent probe **B**. The noted rise in NAD(P)H levels post-TLR4 activation reflects metabolic shifts toward glycolysis and increased cellular respiration, characteristic of immune cell activation in response to stimuli. The sensitivity of fluorescent probe **B** enabled real-time detection and quantification of these metabolic changes, offering critical insights into the metabolic dynamics of immune cells in response to TLR4-mediated signaling, with implications for understanding and potentially modulating immune responses in various pathological conditions. These coenzymes are indispensable to cellular redox functions, antioxidant defenses, and energy metabolism. TLR4 signaling pathways, including NF-κB and MAPK cascades, regulate metabolic enzyme activity related to NAD(P)H metabolism.[64,65] The heightened NAD(P)H levels reflect the metabolic reprogramming necessary to support the energetic demands and redox balance required for immune responses triggered by TLR4 activation.

3.6. Fluorescence Imaging of NAD(P)H in Kidney Tissues. Autosomal dominant polycystic kidney disease (ADPKD) is distinguished by complex pathophysiological features that lead to reprogrammed metabolisms.[66−68] These conditions often involve dysregulated cellular processes such as enhanced glycolysis, mitochondrial dysfunction, oxidative stress, inflammation, and hypoxia. These metabolic alterations contribute to elevated levels of NAD and NADP in affected kidney tissues, reflecting profound shifts in cellular energetics and redox balance.[66−68] In this study, fluorescent probe **B** was employed to investigate NAD(P)H levels in the kidneys of ADPKD mice and patients. Specifically, we evaluated the renal levels of NAD(P)H in 5 week-old phenotypic wildtype (WT, $Pkd1^{RC/+}$) and ADPKD ($Pkd1^{RC/RC}$) mice. We found that normal kidneys of WT mice exhibited faint fluorescence, indicating lower NAD(P)H levels, whereas cystic kidneys of ADPKD mice displayed significantly stronger fluorescence, suggesting enhanced NAD(P)H levels in ADPKD in comparison to their normal counterparts (Figure 13). Consistently, we found a higher level of NAD(P)H in the kidneys of human ADPKD compared with sex- and age-matched normal human kidneys (NHK) (Figure 14). These observations highlighted the potential of probe **B** to uncover metabolic disparities associated with kidney diseases, providing critical insights into disease mechanisms and potential therapeutic targets. By elucidating these metabolic alterations, this study advances the comprehension of renal pathophysiology and lays the groundwork for implementing focused treatments to restore metabolic homeostasis and improve clinical outcomes for patients with kidney disorders. It helps to build the foundation for targeted interventions that restore metabolic homeostasis and improve clinical discoveries in patients with kidney diseases.

3.7. Fluorescence Fruit Fly Larva Imaging for NAD(P)H Detection. Fruit fly larvae (freshly hatched) already exposed to a period of starvation were employed to assess probe **B**'s effectiveness in monitoring dynamic changes in NAD(P)H levels in vivo. The larvae are an ideal model organism because of their stable NAD(P)H levels, which are maintained through metabolic adjustments to nutrient deprivation immediately after hatching.[26,31−33] During starvation, larvae exhibit robust conservation of NAD(P)H, an important coenzyme in metabolic functions, establishing a reliable baseline for studying NAD(P)H variations responding to experimental manipulations. PBS solution-immersed control

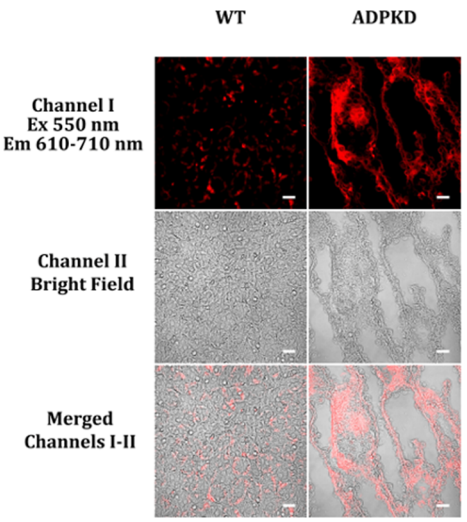

Figure 13. Emission images of wild-type (WT) and ADPKD (autosomal dominant polycystic kidney disease) mouse kidney tissues. Kidney tissue sections of 5 week-old phenotypic WT ($Pkd1^{RC/+}$) and ADPKD ($Pkd1^{RC/RC}$) mice that underwent deparaffinization and rehydration with a subsequent incubation of 5 μM probe **B** for 20 min. Emission was under a 550 nm excitation, and emissions were gathered from 610 to 710 nm. The scale bar signifies 50 μm.

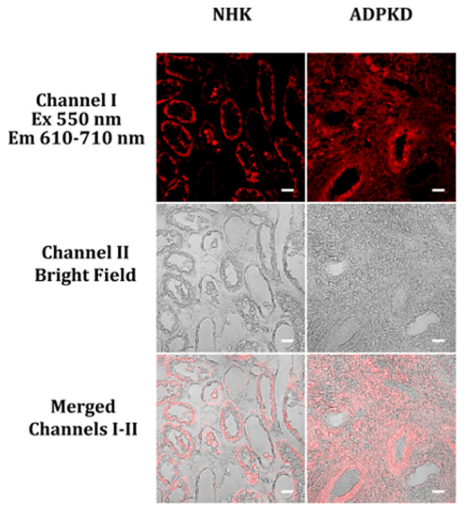

Figure 14. Emission images of NHK and ADPKD (autosomal dominant polycystic kidney disease) human kidney tissues, with a subsequent incubation of 5 μM probe **B** for 20 min. Emission was under a 550 nm excitation, and emissions were gathered from 610 to 710 nm. The scale bar signifies 50 μm.

larvae with probe **B** exhibited minimal fluorescence, validating the identification of NAD(P)H baseline values. Subsequent exposure of these larvae to altering concentrations of NADH resulted in a dose-related augmentation of emission intensity, representing enhanced NAD(P)H levels (Figure 15). This underscores probe **B**'s high sensitivity in detecting in vivo changes in NAD(P)H levels responding to exogenously applied NADH.

4. CONCLUSIONS

In summary, the development of probes **A** and **B**, deep-red and NIR compact cyanine dyes, marks a significant leap forward in mitochondrial NAD(P)H measurement. These probes feature a unique structural design that enhances their fluorescence

https://doi.org/10.1021/acsabm.4c01345
ACS Appl. Bio Mater. 2024, 7, 8552−8564

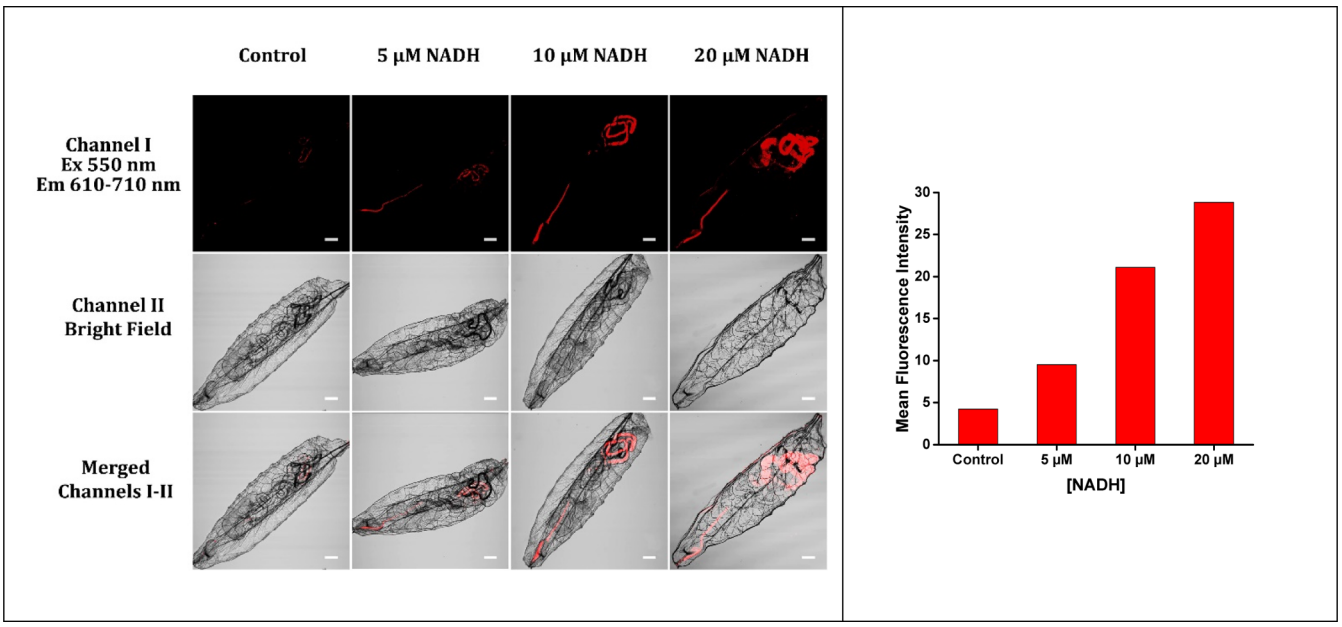

Figure 15. Emission image of fruit fly larva showcasing the effect of different NADH levels on the larva. The larva was treated for 30 min with the respective NADH concentrations with a subsequent incubation of 10 μM probe **B** for 20 min. Emission was under a 550 nm excitation, and emission signals were gathered from 610 to 710 nm. Scale bar: 200 μm.

behavior in the presence of NAD(P)H, effectively addressing issues like delayed responses seen with traditional near-infrared cyanine dyes with significantly extended π-conjugations. Notably, probe **B**, distinguished by its near-infrared emission and rapid detection kinetics, emerged as a standout in monitoring dynamic NAD(P)H levels across diverse biological and pathological scenarios. Our experimental findings demonstrate probe **B**'s precision in detecting NAD(P)H fluctuations induced by chemical stimuli such as Ace-K exposure, cisplatin treatment, $CoCl_2$-induced hypoxia, and TLR4 activation in macrophages. Furthermore, its application in disease models underscored its sensitivity to metabolic changes associated with kidney pathology and its suitability for in vivo investigations, as evidenced by successful monitoring in fruit fly larvae under starvation conditions. Overall, probe **B**'s robust performance highlights its potential as a versatile tool for real-time assessment of mitochondrial function and cellular metabolism.

■ ASSOCIATED CONTENT

Supporting Information

The Supporting Information is available free of charge at https://pubs.acs.org/doi/10.1021/acsabm.4c01345.

Detailed methods and results including synthesis, spectral analysis, and biological assays as well as supporting graphical and statistical data (PDF)

■ AUTHOR INFORMATION

Corresponding Authors

Adonis Amoli − *Department of Chemistry and Health Research Institute, Michigan Technological University, Houghton, Michigan 49931, United States*; Email: aamoli@mtu.edu

Yan Zhang − *Health Research Institute and Department of Biological Sciences, Michigan Technological University, Houghton, Michigan 49931, United States*; Email: yzhang49@mtu.edu

Athar Ata − *Department of Chemistry and Health Research Institute, Michigan Technological University, Houghton, Michigan 49931, United States*; Email: aata@mtu.edu

Haiying Liu − *Department of Chemistry and Health Research Institute, Michigan Technological University, Houghton, Michigan 49931, United States*; orcid.org/0000-0001-8351-2017; Email: hyliu@mtu.edu

Authors

Mahmood Norouzi − *Department of Chemistry and Health Research Institute, Michigan Technological University, Houghton, Michigan 49931, United States*

Yang Zhang − *Health Research Institute and Department of Biological Sciences, Michigan Technological University, Houghton, Michigan 49931, United States*

Ashlyn Colleen Beatty − *Health Research Institute and Department of Biological Sciences, Michigan Technological University, Houghton, Michigan 49931, United States*

Anna Jarvi − *Health Research Institute and Department of Biological Sciences, Michigan Technological University, Houghton, Michigan 49931, United States*

Thomas Werner − *Health Research Institute and Department of Biological Sciences, Michigan Technological University, Houghton, Michigan 49931, United States*

Complete contact information is available at: https://pubs.acs.org/10.1021/acsabm.4c01345

Notes

The authors declare no competing financial interest.

■ ACKNOWLEDGMENTS

The current research received support from multiple sources. The National Institute of Diabetes and Digestive and Kidney Diseases (award number R15DK137195) and the PKD Foundation (Grant 1021264) provided funding for Y. Zhang.

Additionally, Y. Zhang is grateful for the National Science Foundation's financial assistance under award number 2117318. We also appreciate the Kansas PKD Research and Translation Core Center at the University of Kansas Medical Center (U54D126126) and the Polycystic Kidney Disease Research Resource Consortium (PKD-RRC) for supplying valuable kidney sections of human ADPKD and NHK. Furthermore, this research was enabled by the support provided by multiple organizations. The National Institute of General Medical Sciences, National Institutes of Health, funded our work through award numbers 2R15GM114751, R15GM114751, and R15 GM146206-01 for H. Liu. The crucial support from these organizations was key to the successful outcome of this study, and we are thankful for their role in advancing research and scientific knowledge in this area. We also extend our sincere thanks to the National Science Foundation for their financial support through award number 2117318. This funding enabled the purchase of a new NMR spectrometer, which was crucial for characterizing the chemical structures of the fluorescent probes. H. Liu was a recipient of this grant.

REFERENCES

(1) Kluge, M. A.; Fetterman, J. L.; Vita, J. A. Mitochondria and Endothelial Function. *Circ. Res.* **2013**, *112* (8), 1171−1188.
(2) Tang, X. Q.; Luo, Y. X.; Chen, H. Z.; Liu, D. P. Mitochondria, endothelial cell function, and vascular diseases. *Front. Physiol.* **2014**, *5*, 175.
(3) Ying, W. H. NAD^+ and NADH in cellular functions and cell death. *Front. Biosci.* **2006**, *11*, 3129−3148.
(4) Ying, W. H. NAD^+ and NADH in brain functions, brain diseases and brain aging. *Front. Biosci.* **2007**, *12*, 1863−1888.
(5) Yan, L. J. NADH/NAD^+ Redox Imbalance and Diabetic Kidney Disease. *Biomolecules* **2021**, *11* (5), 730.
(6) Shen, G. X. Oxidative stress and diabetic cardiovascular disorders: roles of mitochondria and NADPH oxidaseThis review is one of a selection of papers published in a Special Issue on Oxidative Stress in Health and Disease. *Can. J. Physiol. Pharmacol.* **2010**, *88* (3), 241−248.
(7) Belarbi, K.; Cuvelier, E.; Destée, A.; Gressier, B.; Chartier-Harlin, M. C. NADPH oxidases in Parkinson's disease: a systematic review. *Mol. Neurodegener.* **2017**, *12*, 84.
(8) Fukai, T.; Ushio-Fukai, M. Cross-Talk between NADPH Oxidase and Mitochondria: Role in ROS Signaling and Angiogenesis. *Cells* **2020**, *9* (8), 1849.
(9) Ying, W. H. NAD+ and NADH in brain functions, brain diseases and brain aging. *Front. Biosci.* **2007**, *12*, 1863−1888.
(10) Yan, L. J. NADH/NAD^+ Redox Imbalance and Diabetic Kidney Disease. *Biomolecules* **2021**, *11* (5), 730.
(11) Li, Y.; Zhou, Y. M.; Yue, X. L.; Dai, Z. F. Cyanine Conjugate-Based Biomedical Imaging Probes. *Adv. Healthcare Mater.* **2020**, *9* (22), No. e2001327.
(12) Ilina, K.; Henary, M. Cyanine Dyes Containing Quinoline Moieties: History, Synthesis, Optical Properties, and Applications. *Chem.—Eur. J.* **2021**, *27* (13), 4230−4248.
(13) Zhou, H. J.; Ren, T. B. Recent Progress of Cyanine Fluorophores for NIR-II Sensing and Imaging. *Chem.—Asian J.* **2022**, *17* (8), No. e202200147.
(14) Ding, C. P.; Ren, T. B. Near infrared fluorescent probes for detecting and imaging active small molecules. *Coord. Chem. Rev.* **2023**, *482*, 215080.
(15) Li, X. C.; Zhao, Y. P.; Yin, J. L.; Lin, W. Y. Organic fluorescent probes for detecting mitochondrial membrane potential. *Coord. Chem. Rev.* **2020**, *420*, 213419.
(16) Xiao, H. B.; Li, P.; Tang, B. Recent progresses in fluorescent probes for detection of polarity. *Coord. Chem. Rev.* **2021**, *427*, 213582.
(17) Huang, Y. F.; Liang, J. P.; Fan, Z. F. A review: Small organic molecule dual/multi-organelle-targeted fluorescent probes. *Talanta* **2023**, *259*, 124529.
(18) Podder, A.; Koo, S.; Lee, J.; Mun, S.; Khatun, S.; Kang, H. G.; Bhuniya, S.; Kim, J. S. A rhodamine based fluorescent probe validates substrate and cellular hypoxia specific NADH expression. *Chem. Commun.* **2019**, *55* (4), 537−540.
(19) Podder, A.; Murali, V. P.; Deepika, S.; Dhamija, A.; Biswas, S.; Maiti, K. K.; Bhuniya, S. NADH-Activated Dual-Channel Fluorescent Probes for Multicolor Labeling of Live Cells and Tumor Mimic Spheroids. *Anal. Chem.* **2020**, *92* (18), 12356−12362.
(20) Podder, A.; Thirumalaivasan, N.; Chao, Y. K.; Kukutla, P.; Wu, S. P.; Bhuniya, S. Two-photon active fluorescent indicator for detecting NADH dynamics in live cells and tumor tissue. *Sens. Actuators, B* **2020**, *324*, 128637.
(21) Li, M. Z.; Liu, C.; Zhang, W. J.; Xu, L. F.; Yang, M. M.; Chen, Z. L.; Wang, X. X.; Pu, L. L.; Liu, W. L.; Zeng, X. S.; et al. An NADH-selective and sensitive fluorescence probe to evaluate living cell hypoxic stress. *J. Mater. Chem. B* **2021**, *9* (46), 9547−9552.
(22) Park, S. Y.; Yoon, S. A.; Cha, Y. J.; Lee, M. H. Recent advances in fluorescent probes for cellular antioxidants: Detection of NADH, hNQO1, H_2S, and other redox biomolecules. *Coord. Chem. Rev.* **2021**, *428*, 213613.
(23) Sun, P. J.; Zhang, H. X.; Sun, Y. Q.; Liu, J. The recent development of fluorescent probes for the detection of NADH and NADPH in living cells and in vivo. *Spectrochim. Acta, Part A* **2021**, *245*, 118919.
(24) Zhang, Y. B.; Arachchige, D. L.; Olowolagba, A.; Luck, R. L.; Liu, H. Y. Near-infrared fluorescent probe based on rhodamine derivative for detection of NADH in live cells. *Methods* **2022**, *204*, 22−28.
(25) Wang, Q.; Zhu, Y. Z.; Chen, D. B.; Ou, J. L.; Chen, M.; Feng, Y.; Wang, W. B.; Meng, X. M. A dual-salt fluorescent probe for specific recognition of mitochondrial NADH and potential cancer diagnosis. *Talanta* **2023**, *257*, 124393.
(26) Dwivedi, S. K.; Arachchige, D. L.; Waters, M.; Jaeger, S.; Mahmoud, M.; Olowolagba, A. M.; Tucker, D. R.; Geborkoff, M. R.; Werner, T.; Luck, R. L.; et al. Near-infrared absorption and emission probes with optimal connection bridges for live monitoring of NAD(P)H dynamics in living systems. *Sens. Actuators, B* **2024**, *402*, 135073.
(27) Sun, Y. X.; Mao, Y. Y.; Bai, T. W.; Ye, T. Q.; Lin, Y. F.; Wang, F.; Li, L.; Guo, L. H.; Liu, H. Y.; Wang, J. B. An activated near-infrared mitochondrion-targetable fluorescent probe for rapid detection of NADH. *Chem. Commun.* **2024**, *60* (46), 5932−5935.
(28) Zhao, Y. H.; Wei, K. Y.; Kong, F. P.; Gao, X. N.; Xu, K. H.; Tang, B. Dicyanoisophorone-Based Near-Infrared-Emission Fluorescent Probe for Detecting NAD(P)H in Living Cells and in Vivo. *Anal. Chem.* **2019**, *91* (2), 1368−1374.
(29) Joo, J. H.; Won, M.; Park, S. Y.; Park, K.; Shin, D. S.; Kim, J. S.; Lee, M. H. A dicyanocoumarin-fused quinolinium based probe for NAD(P)H and its use for detecting glycolysis and hypoxia in living cells and tumor spheroids. *Sens. Actuators, B* **2020**, *320*, 128360.
(30) Olowolagba, A. M.; Idowu, M. O.; Arachchige, D. L.; Aworinde, O. R.; Dwivedi, S. K.; Graham, O. R.; Werner, T.; Luck, R. L.; Liu, H. Y. Syntheses and Applications of Coumarin-Derived Fluorescent Probes for Real-Time Monitoring of NAD(P)H Dynamics in Living Cells across Diverse Chemical Environments. *ACS Appl. Bio Mater.* **2024**, *7* (8), 5437−5451.
(31) Arachchige, D. L.; Dwivedi, S. K.; Jaeger, S.; Olowolagba, A. M.; Mahmoud, M.; Tucker, D. R.; Fritz, D. R.; Werner, T.; Tanasova, M.; Luck, R. L.; et al. Highly Sensitive Cyanine Dyes for Rapid Sensing of NAD(P)H in Mitochondria and First-Instar Larvae of Drosophila melanogaster. *ACS Appl. Bio Mater.* **2023**, *6* (8), 3199−3212.
(32) Dwivedi, S. K.; Arachchige, D. L.; Olowolagba, A.; Mahmoud, M.; Cunnien, J.; Tucker, D. R.; Fritz, D.; Werner, T.; Luck, R. L.; Liu, H. Y. Thiophene-based organic dye with large Stokes shift and deep

https://doi.org/10.1021/acsabm.4c01345
ACS Appl. Bio Mater. 2024, 7, 8552−8564

red emission for live cell NAD(P)H detection under varying chemical stimuli. *J. Mater. Chem. B* **2023**, *11* (27), 6296−6307.
(33) Arachchige, D. L.; Dwivedi, S. K.; Waters, M.; Jaeger, S.; Peters, J.; Tucker, D. R.; Geborkoff, M.; Werner, T.; Luck, R. L.; Godugu, B.; et al. Sensitive monitoring of NAD(P)H levels within cancer cells using mitochondria-targeted near-infrared cyanine dyes with optimized electron-withdrawing acceptors. *J. Mater. Chem. B* **2024**, *12* (2), 448−465.
(34) Xia, S.; Zhang, Y. B.; Fang, M. X.; Mikesell, L.; Steenwinkel, T. E.; Wan, S. L.; Phillips, T.; Luck, R. L.; Werner, T.; Liu, H. Y. A FRET-Based Near-Infrared Fluorescent Probe for Ratiometric Detection of Cysteine in Mitochondria. *ChemBioChem* **2019**, *20* (15), 1986−1994.
(35) Zhang, Y. B.; Yan, Y. N.; Xia, S.; Wan, S. L.; Steenwinkel, T. E.; Medford, J.; Durocher, E.; Luck, R. L.; Werner, T.; Liu, H. Y. Cell Membrane-Specific Fluorescent Probe Featuring Dual and Aggregation-Induced Emissions. *ACS Appl. Mater. Interfaces* **2020**, *12* (18), 20172−20179.
(36) Mazi, W.; Yan, Y. N.; Zhang, Y. B.; Xia, S.; Wan, S. L.; Tajiri, M.; Luck, R. L.; Liu, H. Y. A near-infrared fluorescent probe based on a hemicyanine dye with an oxazolidine switch for mitochondrial pH detection. *J. Mater. Chem. B* **2021**, *9* (3), 857−863.
(37) Wan, S. L.; Xia, S.; Medford, J.; Durocher, E.; Steenwinkel, T. E.; Rule, L.; Zhang, Y. B.; Luck, R. L.; Werner, T.; Liu, H. Y. A ratiometric near-infrared fluorescent probe based on a novel reactive cyanine platform for mitochondrial pH detection. *J. Mater. Chem. B* **2021**, *9* (25), 5150−5161.
(38) Yan, Y. N.; Zhang, Y. B.; Xia, S.; Wan, S. L.; Vohs, T.; Tanasova, M.; Luck, R. L.; Liu, H. Y. Ratiometric Near-Infrared Fluorescent Probes Based on Hemicyanine Dyes Bearing Dithioacetal and Formal Residues for pH Detection in Mitochondria. *Molecules* **2021**, *26* (7), 2088.
(39) Wan, S. L.; Vohs, T.; Steenwinkel, T. E.; White, W. R.; Lara-Ramirez, A.; Luck, R. L.; Werner, T.; Tanasova, M.; Liu, H. Y. Near-Infrared Fluorescent Probes with Amine-Incorporated Xanthene Platforms for the Detection of Hypoxia. *ACS Appl. Bio Mater.* **2022**, *5* (9), 4294−4300.
(40) Zhang, Y. B.; Hu, J.; Rong, X. Q.; Jiang, J.; Wang, Y.; Zhang, X. T.; Xu, Z. H.; Xu, K.; Wu, M.; Fang, M. X. Development of a hybrid rhodamine-hydrazine NIR fluorescent probe for sensitive detection and imaging of peroxynitrite in necrotizing enterocolitis model. *Bioorg. Chem.* **2024**, *152*, 107729.
(41) Shang, J. T.; Zhang, Y. Y.; Cheng, Y. T.; Wang, B. L.; Rong, X. Q.; Zhang, Y. B.; Gao, W.; Fang, M. X. Development of a novel Near-Infrared fluorescent probe based on rhodamine derivative for highly selective and sensitive detection of phosgene. *Microchem. J.* **2024**, *196*, 109653.
(42) Zhang, Y. B.; Wang, S. C.; Sun, Y.; Xu, H. B.; Xu, Z. H.; Liang, X.; Yang, J. G.; Song, W. Y.; Chen, M. H.; Fang, M. X. Evaluation of a biomarker (NO) dynamics in inflammatory zebrafish and periodontitis saliva samples via a fast-response and sensitive fluorescent probe. *Bioorg. Chem.* **2024**, *143*, 107014.
(43) Karstadt, M. L. Regulation of carcinogenic food additives in the United States. *Eur. J. Oncol.* **2009**, *14* (2), 79−92.
(44) Magnuson, B. A.; Carakostas, M. C.; Moore, N. H.; Poulos, S. P.; Renwick, A. G. Biological fate of low-calorie sweeteners. *Nutr. Rev.* **2016**, *74* (11), 670−689.
(45) Çelik Atalay, E.; Demirhan, B. E.; Celep, A. G. S. Low-Calorie Sweeteners and Reproductive Health: Evidence and Debates. *Curr. Nutr. Food Sci.* **2024**, *21* (3), 309−332.
(46) Park, S.; Sethi, S.; Bouret, S. G. Non-nutritive Sweeteners Induce Hypothalamic ER Stress Causing Abnormal Axon Outgrowth. *Front. Endocrinol.* **2019**, *10*, 876.
(47) Sylvetsky, A. C.; Sen, S.; Merkel, P.; Dore, F.; Stern, D. B.; Henry, C. J.; Cai, H.; Walter, P. J.; Crandall, K. A.; Rother, K. I.; et al. Consumption of Diet Soda Sweetened with Sucralose and Acesulfame-Potassium Alters Inflammatory Transcriptome Pathways in Females with Overweight and Obesity. *Mol. Nutr. Food Res.* **2020**, *64* (11), No. e1901166.
(48) Chiang, Y. F.; Chen, H. Y.; Lai, Y. H.; Ali, M.; Chen, Y. C.; Hsia, S. M. Consumption of Artificial Sweetener Acesulfame Potassium Increases Preterm Risk and Uterine Contraction with Calcium Influx Increased via Myosin Light Chain Kinase-Myosin Light Chain 20 Related Signaling Pathway. *Mol. Nutr. Food Res.* **2022**, *66* (20), No. e2200298.
(49) Yao, X.; Panichpisal, K.; Kurtzman, N.; Nugent, K. Cisplatin nephrotoxicity: A review. *Am. J. Med. Sci.* **2007**, *334* (2), 115−124.
(50) Barabas, K.; Milner, R.; Lurie, D.; Adin, C. Cisplatin: a review of toxicities and therapeutic applications. *Vet. Comp. Oncol.* **2008**, *6* (1), 1−18.
(51) Li, Y. R.; Zhang, T. Y.; Song, Q.; Gao, D. K.; Li, Y.; Jie, H. Q.; Huang, P.; Zheng, G. L.; Yang, J.; He, J. C. Cisplatin ototoxicity mechanism and antagonistic intervention strategy: a scope review. *Front. Cell. Neurosci.* **2023**, *17*, 1197051.
(52) Vermorken, J. B.; Huinink, W. W. T.; Eisenhauer, E. A.; Favalli, G.; Belpomme, D.; Conte, P. F.; Kaye, S. B. Carboplatin Versus Cisplatin. *Ann. Oncol.* **1993**, *4*, 41−48.
(53) Auselo, N. M.; Bonsrosset, F.; Pellaecosset, B.; Costa, P.; Schwartz, Y.; Louis, J. F.; Navratil, H. Carboplatin And Urothelial Tumors - An Overview. *Bull. Cancer* **1995**, *82* (3), 181−188.
(54) Rose, P. G.; Fusco, N.; Fluellen, L.; Rodriguez, M. Carboplatin hypersensitivity reactions in patients with ovarian and peritoneal carcinoma. *International Journal of Gynecological Cancer* **1998**, *8* (5), 365−368.
(55) Ruggiero, A.; Rizzo, D.; Catalano, M.; Attinà, G.; Riccardi, R. Hypersensitivity to Carboplatin in Children with Malignancy. *Front. Pharmacol* **2017**, *08*, 201.
(56) Dinnes, J.; Cave, C.; Huang, S.; Milne, R. A rapid and systematic review of the effectiveness of Temozolomide for the treatment of recurrent malignant glioma. *Br. J. Cancer* **2002**, *86* (4), 501−505.
(57) Quirt, I.; Verma, S.; Petrella, T.; Bak, K.; Charette, M. Temozolomide for the treatment of metastatic melanoma: A systematic review. *Oncologist* **2007**, *12* (9), 1114−1123.
(58) Dresemann, G. Temozolomide in malignant glioma. *OncoTargets Ther.* **2010**, *3*, 139−146.
(59) Ortiz, L. D.; Syro, L. V.; Scheithauer, B. W.; Rotondo, F.; Uribe, H.; Fadul, C. E.; Horvath, E.; Kovacs, K. Temozolomide in aggressive pituitary adenomas and carcinomas. *Clinics* **2012**, *67*, 119−123.
(60) Arvelo, F.; Cotte, C. Hypoxia in cancer malignity. Review. *Invest. Clin.* **2009**, *50* (4), 529−546.
(61) Debenham, M. I. B.; Smuin, J. N.; Grantham, T. D. A.; Ainslie, P. N.; Dalton, B. H. Hypoxia and standing balance. *Eur. J. Appl. Physiol.* **2021**, *121* (4), 993−1008.
(62) Piret, J. P.; Mottet, D.; Raes, M.; Michiels, C. CoCl2, a chemical inducer of hypoxia-inducible factor-1, and hypoxia reduce apoptotic cell death in hepatoma cell line HepG2. In *Cell Signaling, Transcription, and Translation as Therapeutic Targets*; Diederich, M., Ed., 2002; Vol. *973*, pp 443−447.*Annals of the New York Academy of Sciences*
(63) Borenstein, X.; Fiszman, G. L.; Blidner, A.; Vanzulli, S. I.; Jasnis, M. A. Functional changes in murine mammary cancer cells elicited by $CoCl_2$-induced hypoxia. *Nitric Oxide-Biology and Chemistry* **2010**, *23* (3), 234−241.
(64) Rivas-Santiago, B.; Juárez, E. Toll-like receptor in lung response to pathogens. *Revista De Investigacion Clinica-Clinical and Translational Investigation* **2007**, *59* (6), 481−488.
(65) Wagner, H. Toll-Like Receptors in Gastrointestinal Diseases. *Digestive Diseases* **2012**, *30*, 74−77.
(66) Niemczyk, M.; Niemczyk, S.; Paczek, L. Autosomal dominant polycystic kidney disease and transplantation. *Ann. Transplant.* **2009**, *14* (4), 86−90.
(67) Torra, R. Treatment of autosomal dominant polycystic kidney disease. *Med. Clin.* **2014**, *142* (2), 73−79.
(68) Cadnapaphornchai, M. A. Clinical Trials in Pediatric Autosomal Dominant Polycystic Kidney Disease. *Front. Pediatr.* **2017**, *5*, 53.

https://doi.org/10.1021/acsabm.4c01345
ACS Appl. Bio Mater. 2024, 7, 8552−8564